The influence of electrospun fibre size on Schwann cell behaviour and axonal outgrowth

The influence of electrospun fibres size on Schwann cells behaviour and axonal outgrowth.

Gnavi S. [a,b], Fornasari B.E.[a,b], Tonda-Turo C.[c], Ciardelli G.[c,d], Zanetti M.[e], Geuna S.[a,b]* and Perroteau I.[a]

[a] Department of Clinical and Biological Sciences, University of Torino, Orbassano, 10043, Italy; isabelle.perroteau@unito.it

[b] Neuroscience Institute of the Cavalieri-Ottolenghi Foundation, University of Torino, Orbassano, 10043, Italy; sara.gnavi@unito.it; benedetta.fornasari@gmail.com; stefano.geuna@unito.it

[c] Politecnico di Torino, Department of Mechanical and Aerospace Engineering, Politecnico of Torino, Torino, 10100 Italy; chiara.tondaturo@polito.it

[d] CNR-IPCF UOS, Pisa, 56124, Italy; gianluca.ciardelli@polito.it

[e] Nanostructured Interfaces and Surfaces, Department of Chemistry, University of Torino, Torino, 10100 Italy; marco.zanetti@unito.it

*Corresponding author:

Stefano Geuna, MD

Ospedale San Luigi, Department of Clinical and Biological Sciences

Regione Gonzole 10, 10043 - Orbassano (TO) – ITALY

tel (+39) 011.670.5433/36

fax (+39) 011.903.8639

e-mail: stefano.geuna@unito.it

ABSTRACT

Fibrous substrates, functioning as a temporary extracellular matrix, can be easily prepared by electrospinning which allows to obtain fibrous matrices suitable as internal filler for nerve guidance channels. In this study, gelatin micro- or nano-fibres have been prepared by electrospinning technique by tuning gelatin concentration and solution flow rate. The influence of gelatin fibre diameter on cell adhesion and proliferation was tested *in vitro* using Schwann cells (SC) and dorsal root ganglia (DRG) explant cultures. Cell adhesion was evaluated by quantifying cell spreading area, actin cytoskeleton organization and focal adhesion complex formation. Nano-fibres showed to promote cell spreading and actin cytoskeleton organization, resulting in higher cellular adhesion and proliferation rate. Yet, cell migration and motility were quantified by transwell and time lapse assays respectively and results showed that cells cultured on micro-fibres displayed higher motility and migration rate. Finally, DRG axon outgrowth resulted to be higher on micro-fibres. These data suggest that gelatin electrospun fibres topography can be adjusted in order to modulate SC and axons organization and that both nano- and micro-fibres are promising fillers for the design of devices for peripheral nerve repair.

KEYWORDS electrospun fibres, extracellular matrix, cell adhesion, cell spreading, axon outgrowth, nerve tissue engineering

1. INTRODUCTION

In recent years, a considerable body of research has focused on the development of implantable polymeric scaffolds to be used in the repair of nerve gaps as alternative to autograft [1-5]. The need of artificial scaffolds for nerve tissue engineering comes from the limited autologous nerve availability and the requirement of secondary surgery that may result in donor sensory loss and/or pain when using nerve autografts-based technique, and from the immune-rejection problems common to allografts- and xenografts-based techniques [6-9].

Biomimetic materials for peripheral nerve reconstruction should: be biodegradable and biocompatible, display a large surface area and high porosity and provide adequate mechanical support for re-growing axons. To achieve these goals, scaffold for peripheral nerve repair can be functionalized by acting on the properties of the inner filler [1, 6, 10, 11] in order to mimic the native structure of the nerve and to enhance nerve repair processes [12-14]. First, the inner filler three-dimensional-structure architecture (topography) and second, the biochemical composition have to be taken in consideration for the development of innovative implantable nerve scaffolds since these features deeply influence cell behaviour and organization of the regeneration tissue. In particular, the conduit internal filler (i.e. fibre composition, diameter, three dimensional structure, etc.) can be diversified in order to modulate SC and axon behaviour (cell proliferation rate, amount of migrated cells, amount of re-growing axons, etc.).

As concerning the inner filler three-dimensional-structure architecture the basal lamina and the extracellular matrix (ECM) structure have to be taken in consideration.

Tissue basal lamina membrane displays unique nano-fibrous characteristic, suggesting the importance of substrate topography [12-15]. A number of studies demonstrates that micro-to-nano scale topography plays an important role in the controll of adhesion, proliferation and survival of different cell types among them: human cord blood derived hemapoietic stem progenitor cells [16,

17], bone marrow derived osteoprogenitors [18, 19], mesenchymal stem cells [20], MC3T3-E1 preosteoblast cells [17], hippocampal progenitor cells [21], human keratinocytes [22], neural stem cells [23], Schwann cells (SC) [24, 25] and neurons [26, 27].

Surface modification of biomaterial, roughness, porosity, and topographical cues such as grooves and ridges or pits and pillars have been shown to influence protein absorption, cell interaction and host response to the material [14, 28]. Topography modifications of implantable devices have been showed to influence cell adhesion, growth and migration by influencing size, shape, and distribution of focal adhesion plaque, actin cytoskeleton reorganization and/or *lamellipodium* and *filopodia* formation though integrin receptor signalling [13, 14, 28-30].

Ideally, a biomimetic scaffold candidate should mimic the native ECM structure and function defining the optimal three-dimensional tissue organization in order to maintain the normal cell organization, viability, invasion, proliferation and differentiation behaviour [12-14].

Electrospinning is a fascinating and widely utilized technique to produce fibres, mimicking the native ECM, from polymer solution of both natural and synthetic origins. Resulting fibres are characterized by high surface to volume ratio, high porosity and enhanced physic-mechanical properties that can be adjusted by manipulating the polymer solution and processing parameters to get fibres with desired morphology and mechanical strength [31]. Electrospun fibres, mimicking the ECM structure, have been used for different applications such as wound healing, drug delivery, enzymes immobilization, filtration and scaffolds tissue engineering in nerve, dura mater, tendon/ligament and tendon-to-bone insertion repair [12, 22, 31-35].

As concerning the biochemical composition, natural polymers are often used because of their high biocompatibility and bio-functional cues improving the overall scaffold cytocompatibility [3, 36, 37]. Collagen, alginate, silk protein, hyaluronic acid, chitosan and others biomaterial have been used for electrospun fibres preparation [3, 31, 36, 37]. Although, ECM-based biomaterials have some use-limitations such as poor mechanical properties and immunogenicity risk [28, 38].

In this work gelatin, a natural polymer obtained by thermal denaturation of collagen has been chosen for random electrospun fibres production due to its advantageous features. In comparison to collagen, which is an animal protein, gelatin is biocompatible, biodegradable and does not induce immune-rejection problems maintaining molecular cues that play key role in regulating cell behavior [38]. Although these properties, the difficulty in dissolving gelatin in water solution at mild temperature (e.g. 37°C) limits its use in biomedical application [38-41]. In a previous work, authors successfully set up a protocol for gelatin electrospun fibres production. Gelatin was dissolved in distilled water avoiding the use of potentially cytotoxic solvents and acidic solutions [39]. Furthermore, to increase gelatin stability in physiological environment γ-glicidoxypropyltrimethoxysilane (GPTMS) was used as cross-linker agent. GPTMS cross-linking has been reported to do not modify fibres matrix morphology and to reduce the gelatin degradation rate in physiological solutions (from few hours to more than 7 days for gelatin and crosslinked gelatin nano-fibres, respectively). Within this study, authors identified the process and solution parameters to be applied for homogenous nano-fibres fabrication. In details, by tuning gelatin solution concentration in the range from 8 to 15 % $w \cdot v^{-1}$, solution flow rate in the range from 8 to 15 $ml \cdot min^{-1}$ and the nozzle collector distance in the range from 7 to 19 cm, electrospun fibres with a diameter size ranging from 200 to 700 nm were obtained. Nano-fibrous substrates biocompatibility was tested by culturing Neonatal Olfactory Bulb Ensheating Cells (NOBEC) on 300 nm size gelatin fibres [39].

Based on the results of the previous study [39], we develope nano-fibrous matrices characterized by different diameters in order to analyze the influence of fibres size on nerve tissue behaviour. Gelatin-GPTMS cross-linked electrospun fibres with a diameter size ranging from 300 nm to 1300 nm were prepared and *in vitro* and *ex vivo* primary SC culture and dorsal root ganglia (DRG) explants were set up in order to study if the micro-to-nano-scale fibres topography can modulate Schwann cells adhesion, proliferation and migration and axonal outgrowth respectively.

2. MATERIALS AND METHODS

2.1 Fibres preparation

Gelatin solution were prepared as previously described [39] . Briefly, gelatin (type A from porcine skin) and GPTMS were supplied by Sigma Aldrich. Gelatin was dissolved in demineralised water at 50°C to obtain the desired solution concentration (15 or 20 % w v^{-1}) and 137 µl of GPTMS were added to the gelatin solution and mixed for 1 h before spinning.

The electrospinning system used for fibre preparation consists of an isothermal chamber equipped with: a high voltage generator (PS/EL30R01.5-22 Glassman High Voltage), providing a voltage of 0 to 30 kV and a current of 0 to 1.5 mA with reversible polarity; a volumetric pump (KDS210 of KD Scientific), an electrode; a mobile syringe support; a syringe and a 1.5 mm thickness flat aluminium collector.

The gelatin solutions (containing 15% or 20% gelatin) were spinned at 50 °C, 30 kV voltage, flow rate of 10 µl min^{-1} or 15 µl min^{-1} and nozzle-collector distance of 15 cm as previously reported [39]. Briefly, 15% gelatin solution was spinned at a flow rate 10 or 15 µl/min in order to obtain fibres displaying 300 and 600 nm diameter size respectively. 20% gelatin solution was spinned at a flow rate 12.5 or 15 µl/min in order to obtain fibres displaying 1000 and 1300 nm diameter size respectively (Fig 1 A).

Electrospun scaffolds were prepared by using a vertical electrospinning set up in order to collect randomly oriented nano- or micro-fibres on glass coverslips.

2.2 Scanning electron microscope analysis

The morphology of the electrospun matrices was analysed using a scanning electron microscope (STANDARD DEVIATION Philips 525 M) at an accelerate voltage of 15 kV. Before analysis, fibre samples were coated with gold using a sputter coater. The STANDARD DEVIATION magnification (6000×) was selected to have 50 µm squared fields, allowing the analysis of the fibres distribution.

Pore and fibre diameters were quantified by analysing SEM micrographs through *ImageJ* software as previously reported [23, 39]. For each fibre type, three images from three different samples were analysed and the pore and fibre diameters were reported as average value ± standard deviation.

2.3 Cell Culture

RT4-D6P2T Schwann cell line and primary SC were grown in a monolayer at 37 °C in a humidified atmosphere of 5% CO_2 air. RT4-D6P2T were purchased from ATCC (American Type Culture Collection, 10801 University Blvd, Manassas, VA 20110-2209) and grown in complete high glucose Dulbecco's modified Eagle's medium (DMEM, Invitrogen) according to the designated ATCC protocol.

SC primary culture were isolated from adult rat sciatic nerve harvested from adult female Wistar rats (Charles River Laboratories, Milan, Italy) weighing approximately 190-220g. All procedures were performed in accordance with the Ethics Committee and the European Communities Council Directive of 24 November 1986 (86/609/ EEC). Adequate measures were taken to minimize pain and discomfort taking into account human endpoints for animal suffering and distress. Sciatic nerves were isolated, cut into 3 mm section and incubated at 37°C 5% CO_2 air in complete medium consisting in low glucose DMEM (Gibco) supplemented with 100 units ml^{-1} penicillin, 0.1 mg ml^{-1} streptomycin, 1 mM sodium pyruvate, 2 mM L-glutamine, 10% heat-inactivated fetal bovine serum (FBS, Invitrogen), 63 ng/ml of glial growth factor (GGF, R&D System) and 10µM of forskolin (Sigma). The medium was changed every 3 days. After 2 week, 2 ml of digestion solution consisting in 0.6 mg/ml of collagenase type IV (Sigma) and 0.5 mg/ml dispase (Invitrogen) were diluted in low glucose complete medium. After 24 h incubation nerves segments were transferred in a 50 ml tube and suspended in 5 ml of low glucose complete medium using a glass Pasteur pipette. The obtained cell suspension was filtrated through a 70 µm cell strainer (Falcon), centrifuged at 900 rpm for 5 minutes, re-suspended in 10 ml of SC complete

medium and seeded on a poly-L-lysine (PLL, Sigma) coated plate. In order to remove contaminating fibroblasts immunodepletion protocol was performed on confluent SC. Briefly, confluent SC were harvested by trypsinization, re-suspended in 500 µl of low glucose complete medium containing mouse anti-rat Thy1.1 antibody diluted 1:500 (Serotec, MCA04G) and incubated 10 minutes at 37°C. 250 µl of fresh rabbit complement (Cederlane Labs) were added and 30 minutes incubation were performed at 37°C. The reaction was blocked by adding 10 ml of low glucose complete medium and 5 minutes centrifugation step was performed at 900 rpm. Resulting pellet was resuspended in low glucose complete medium and seeded on PLL coated plate. Confluent cells were harvested twice a week by trypsinization and seeded at the desired dilution in a new plate.

Before cell seeding, fibres samples were sterilised by overnight (O/N) exposure to UV irradiation (UV lamp Technoscientific Co., wavelength 254nm) and then incubated O/N with complete DMEM.

2.4 Adhesion assay

RT4-D6P2T and primary SC were seeded in complete DMEM at a density of 4000 or 8000 cells/cm^2 on both PLL (control condition) and gelatin-fibres coated coverslips. After 3, 6 or 24 h, culture medium was removed, substrates with attached cells were rinsed with PBS with Ca^{2+} and Mg^{2+} and fixed by incubation with 4% paraformaldehyde solution (PFA, Sigma-Aldrich). After 20 minutes, the PFA solution was removed and samples were rinsed with PBS with Ca^{2+} and Mg^{2+}. Fixed cells were permeabilized with 0.1% Triton X-100 diluted in PBS for 10 minutes at room temperature and blocking solution (normal goat serum, NGS, diluted 1:100 in PBS DAKO X0907) was applied for 1 hour at room temperature. Cells were stained by O/N incubation with anti-S-100β rabbit polyclonal antibody (diluted 1:600 in PBS, Sigma) followed by 1 hour incubation with goat-anti-rabbit IgG (H+L) Cy3 secondary antibody at room temperature (diluted 1:200 in PBS,

Jacknson) or goat-anti rabbit IgG (H+L) AlexaFluor488 (diluted 1:200 in PBS, Invitrogen). Nuclei were stained with 4, 6-diamidino-2-phenylindole (DAPI, Sigma) diluted 1:1000 in PBS.

Cells were photographed by an inverted optical video-confocal microscope (ViCo, Nikon Eclipse 80i) equipped with a Nikon ECLIPSE 80i camera using Image-Pro Plus 6.0 (Media Cybernetics USA). The number of adherent cells was counted with *ImageJ*. The experiments were repeated three times independently and included the use of 5 sets of samples. Each set included 3 fibres matrices and 3 control PLL coated coverslips. For each sample, 30 images were taken at 20X magnification. Cell number and spreading area were calculated using *ImageJ* software. Cell number was analysed, averaged, and expressed as the number of adherent cells/mm^2 ± standard deviation. Spreading area was analysed by calculating the pixel area occupied by cells. Resulting spreading areas were divided by the number of cell quantified for each field, and expressed as pixel area occupied by single cell ± standard deviation.

2.5 Proliferation assay

RT4-D6P2T and primary SC were seeded in complete DMEM at a density of 1000 or 2000 cells/cm^2 on both PLL (control condition) and gelatin-fibres coated coverslips. After 1, 3, 5, and 7 days, cells were fixed, stained, photographed and cell number was evaluated as described in the adhesion assay paragraph. The experiments were repeated three times independently and included the use of 5 sets of samples. For each time interval, 3 fibres matrices and 3 control PLL coating coverslips were used. Number of cells counted for each assays was analysed, averaged, and expressed as number of cells ± standard deviation.

2.6 Actin cytoskeleton organization evaluation

To qualitatively evaluate cell adhesion and morphology, immunocytochemistry analysis was performed. RT4-D6P2T and primary SC were seeded in complete DMEM at a density of 4000 or 8000 cells/cm^2 on both PLL (control condition) and gelatin-fibres coated coverslips. After 3, 6 or 24

h, culture medium was removed, and samples were fixed as described in the adhesion assay paragraph. Fixed cells were permeabilized with 0.1% Triton X-100 in 1X PBS for 10 minutes at room temperature and NGS blocking solution was applied for 1 hour at room temperature as described in the adhesion assay paragraph. F-actin was detected using FITC conjugated phalloidin (diluted 1:1000 in blocking solution, Millipore) by 1 hour incubation at room temperature followed by three wash steps of 5 minutes each. Vinculin was detected by O/N incubation with anti-vinculin mouse monoclonal antibody (diluted 1:100 in PBS, Millipore) followed by 1 hour incubation with goat-anti-mouse IgG (H+L) Alexa 488 secondary antibody (Invitrogen, diluted 1:200 in PBS). Fluorescent images were acquired using an inverted optical video-confocal microscope (ViCo, Nikon Eclipse 80i) equipped with a Nikon ECLIPSE 80i camera using Image-Pro Plus 6.0 (Media Cybernetics USA). The experiments were repeated three times independently and included the use of 5 sets of samples. Each set included 3 fibres matrices and 3 control PLL coated coverslips. The entire procedure was carried out in a blind manner. For each sample 100 cells were examined for a total of 300 cells for each experimental condition. An arbitrary score was given to each cell and data were express as percentage of cells displaying a low, medium or high actin cytoskeleton organization or focal adhesion points presence ± standard deviation.

2.7 Lamellipodium and filopodia evaluation

Lamellipodium and *filopodia* presence was evaluated by direct microscope observation of cells stained with anti-S-100β rabbit polyclonal antibody. Cell staining was performed as described in the adhesion assay paragraph. All images were captured with an inverted optical video-confocal microscope (ViCo, Nikon Eclipse 80i) equipped with a Nikon ECLIPSE 80i camera using Image-Pro Plus 6.0 (Media Cybernetics USA). The experiments were repeated three times independently and included the use of 5 sets of samples. Each set included 3 fibres matrices and 3 control PLL coated coverslips. The entire procedure was carried out in a blind manner. For each sample 100

cells were examined for a total of 300 cells for each experimental condition. Data were expressed as percentage of cells characterized by *lamellipodium* or *filopodia* presence ± standard deviation.

2.8 Bi-dimensional migration assay: time lapse

RT4-D6P2T and primary SC were seeded at a cell density of 4×10^3 cells/cm^2 on the different fibres matrices and control condition and allowed to adhere for 24 hours. Fibres samples were inserted into 24-multiwell plates using CellCrowns (Sigma) to avoid floating of the samples. For time-lapse video recording cells were kept at 37°C, 5% CO_2 in an incubator chamber (Okolab). Cell movements were monitored with an inverted microscope (Eclipse Ti, Nikon) using Plan Fluor10×/0.25 NA objectives (Nikon). Images were collected with CCD video cameras (Roper Scientific) at 30 min time intervals up to 48 hours, digitized and stored as image stacks using MetaMorph 7.6.1.0 software (Universal Imaging Corp.). The experiments were repeated three times independently and included the use of 5 sets of samples. Each set included 3 fibres matrices and 3 control PLL coated condition. 10 cells were analysed for each sample. Image stacks were analysed with the *ImageJ* software using *MtrackJ* plugin. Cell motility was express as μm/sec ± standard deviation.

2.9 Three-dimensional migration assay: transwell assay

10^5 cells suspended in 200 μl of complete DMEM containing 2% FBS were seeded in the upper chamber of a transwell (cell culture insert, BD Biosciences) on a porous transparent polyethylene terephthalate membrane (8.0-μm pore size, 1×10^5 pores/cm^2) on with no fibres matrices (control condition) or the different fibres matrices were inserted using CellCrowns (Scaffdex) to avoid floating of the samples. The lower chamber was filled with complete DMEM medium containing 10% FBS. The 24-well plates containing cell culture inserts were incubated at 37°C in a 5% CO_2/air atmosphere. After 6 h of incubation, cells attached to the upper side of the membrane were mechanically removed using a cotton-tipped applicator. Migrated cells to the lower

side of the membrane were rinsed with PBS, fixed with 2% glutaraldehyde diluted in PBS for 20 minutes at room temperature, washed five times with water, stained with 0.1% crystal violet and 20% methanol for 20 min at room temperature, washed five times with water, air-dried, and photographed using an Nikon ECLIPSE TS100 inverted microscope equipped with a Nikon Digital Sight DSL1 camera; images were analysed with ImageJ software. The experiments were repeated three times independently and include the use of 5 sets of samples. Each set includes 3 control condition transwell and 3 transwell filled with the different fibres matrices. Counted cells were express as percentage of migrated cell/total number of migrated cell ± standard deviation.

2.10 DRG explants

DRG explants were harvested from adult female Wistar rats (Charles River Laboratories, Milan, Italy) weighing approximately 190-220g. DRG explants were cultured on coverslips coated with the different fibres matrices or 100 µl matrigel® in which culture medium without growth factors (negative control), or containing 50 ng NGF/ml (positive control) was added. A total of ten ganglia were mounted per coverslips. After 30 minutes incubation at 37°C, to allow matrigel® or hydrogel polymerization, 2 ml of complete F12-BME medium were added. Complete F12-BME medium consist of F12 and BME medium (Gibco) in 50:50 ratio containing: 1% Bovine Serum Albumin (BSA, Sigma), 0.5 g/ml D-glucose (Sigma), 100U/ml penicillin and streptomycin (Sigma), 1mg/100ml putrescine (Sigma), 2 mM L-glutamine (Sigma), 2 ml of 100X insulin-selenium-transferrin (Gibco) and 0.125 ng/ml vitamin C.

After 48h incubation, explants were fixed with 4% PFA for 20 minutes at RT. Immunocytochemistry, to stain axon, was performed as described in the adhesion assay paragraph using β-tubulin mouse mAb (diluted 1:100, in PBS, Sigma) and goat-anti-mouse IgG (H+L) AlexaFluor488 (diluted 1:200 in PBS, Invitrogen). Nuclei were stained with 4',6-diamidino-2phenylindole (diluted 1:1000 in PBS, Sigma).

The experiments were repeated three times independently and included the use of 5 sets of samples. Each set included 3 fibres matrices and 3 control matrigel® coated coverslips.

For quantification, the whole explants were acquired through an inverted optical video-confocal microscope (ViCo, Nikon Eclipse 80i) equipped with a Nikon ECLIPSE 80i camera using Image-Pro Plus 6.0 (Media Cybernetics USA). Axon density, sprouting area and axon lengths were measured using *ImageJ* software as described elsewhere [42, 43]. Axon density was express as pixel occupied by axon ± standard deviation. Sprouting area was express as DRG axon occupied area/DRG body area ratio ± standard deviation. Axon length was express in μm ± standard deviation.

2.11 Confocal microscopy

Samples were observed with a Nikon Eclipse E800 epifluorescence microscope under appropriate filters and a Leica TCS SP5 confocal laser scanning microscope (Leica, Mannheim, Germany) using a 40× Plan-NEOFLUAR objective (numerical aperture(NA) = 0.50). High resolution images were acquired (1024×1024 pixels) at 100 Hz.

2.12 Statistics

The experiments were repeated three times independently and include the use of 5 sets of samples. Each set includes 3 control condition samples and 3 fibres matrices samples. The data were expressed as mean ± standard deviation. Statistical analysis was carried out using GraphPad Prism® software to execute single-factor analysis of variance (ANOVA). Values of * = $p<0.05$, ** = $p<0.01$,*** = $p<0.001$ were considered as statistically significant.

3. RESULTS

3.1 Increasing gelatin solution concentration and flow rate resulted in fibres production with higher diameter size and porosity

Figure 1 A summarize fibre diameter size and porosity. Increasing gelatin solution concentration and flow rate resulted in increased fibres diameter size and porosity: gelatin solution concentration of 15% and flow rate of 10 µl/min allowed to produce fibres with 340 ± 14 nm, gelatin solution concentration of 15% and flow rate of 15 µl/min allowed the production of fibres with 594 ± 48 nm, gelatin solution concentration of 20% and flow rate of 12,5 µl/min allowed the production of fibres with 1005 ± 20 nm and gelatin solution concentration of 15% and flow rate of 10 µl/min allowed the production of fibres with 1306 ± 34 nm that from now on will be referred as 300 nm fibres, 600 nm fibres, 1000 nm fibres, and 1300 nm fibres.

Figure 1 (B-E) showed representative SEM micrographs of the samples prepared using different process and solution parameters. Pore size of 300 nm fibres was significative lower than the pore size of 600, 1000 nm and 1300 nm fibres.

A

[GL]	Flow rate	Fiber diameter	Porosity	
15%	10 µl/min	340 ± 14 nm	0.182 ± 0.001 µm^2	*** ##
15%	15 µl/min	594 ± 48 nm	0.202 ± 0.004 µm^2	
20%	12,5 µl/min	1005 ± 20 nm	0.208 ± 0.003 µm^2	
20%	15 µl/min	1306 ± 34 nm	0.201 ± 0.003 µm^2	

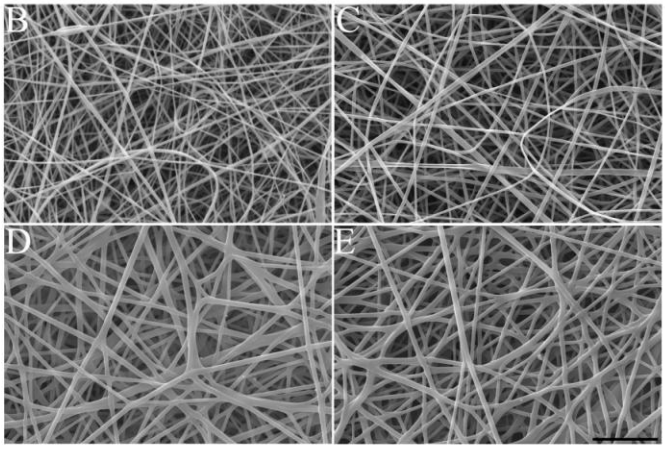

Figure 1. The table reported the varied spinning parameters used for gelatin fibres preparation, fibres diameter size (express in nm ± standard deviation) and porosity measurements (express in µm^2± standard deviation). Statistical analysis was carried out using one-way ANOVA. Asterisks refer to the statistical difference between the porosity rate of 300 nm diameter size fibres in comparison to

the porosity rate of 600 nm and 1000 nm diameter size fibres matrices (***$p \leq 0.001$). Hashes refer to the statistical difference between the porosity rate of 300 nm diameter size fibres in comparison to the porosity rate of 1300 nm diameter size fibres matrices (##$p \leq 0.01$) (A). SEM micrographs of gelatin fibres obtained varying solution concentration and flow rate processing parameter are reported. Gelatin fibres of 300 nm diameter size (B). Gelatin fibres of 600 nm diameter size (C). Gelatin fibres of 1000 nm diameter size (D). Gelatin fibres of 1300 nm diameter size (E).

3.2 Increasing fibre diameter size did not affect the number of adherent cells whereas resulted in cell spreading area decrease

Figures 2 shows the results of the assessment of fibres diameter influence on cell adhesion and morphology of RT4-D6P2T and primary SC cultures. After 3, 6 and 24 hours the number of adherent cells and their morphology were evaluated. Results showed that increasing fibres diameter size did not affect the number of adherent cells for both RT4-D6P2T (Fig. 2P) and primary SC cultures (Fig. 2R).

Increasing fibres diameter size resulted in decreased cell spreading area and elongated cell morphology as evidenced by spreading area quantification (Fig 2 Q and S) and fluorescent microscopy images (Fig.2 A-O). This trend was maintained in all the tested time points (3, 6 and 24 hours). Cells seeded on control condition, 300 and 600 nm fibres displayed a spread morphology in comparison to cells seeded on 1000 and 300 nm fibres which display a more elongated morphology (Fig.2 A-O). Fibre substrates appeared in green due to their auto-fluorescence.

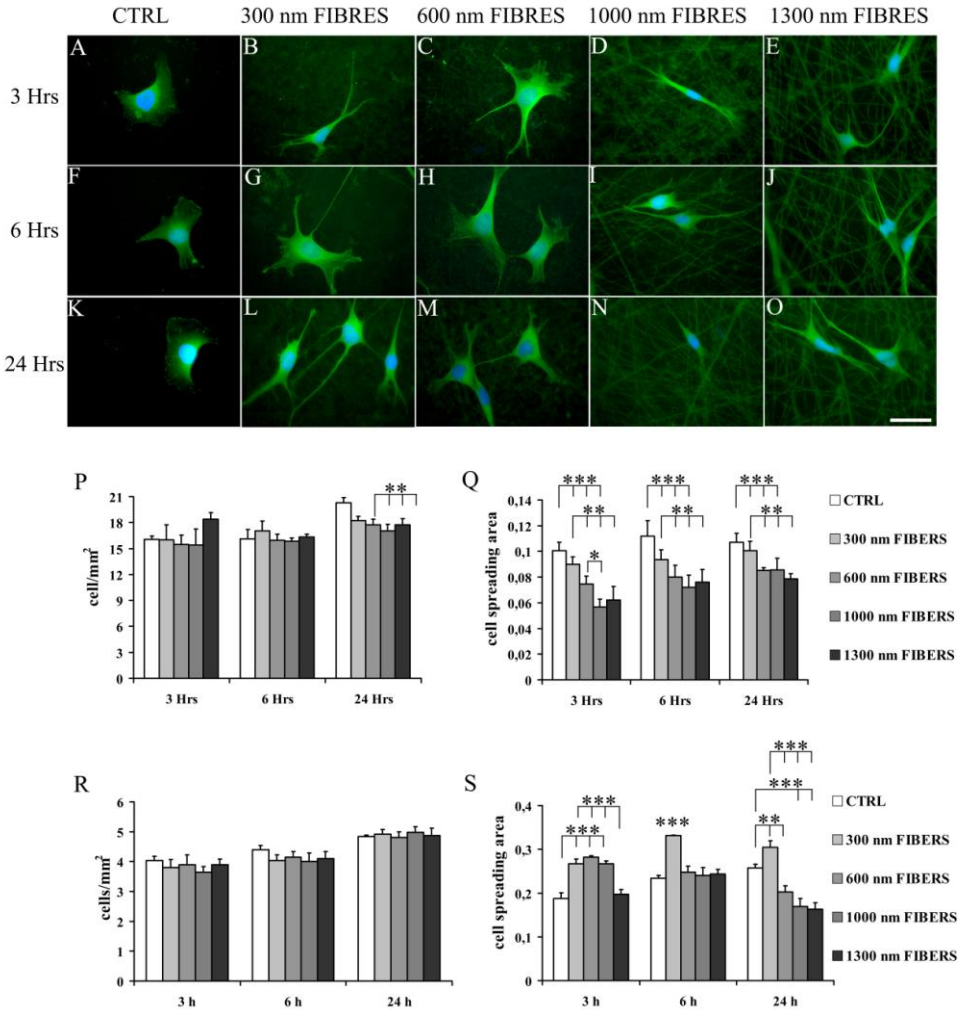

Figure 2. Adhesion assay. Fluorescence images after S100β (green) and DAPI (blue) staining of RT4-D6P2T on poly-L-lysine coated coverslips (control condition, A, F and K), 300 nm diameter size fibres (B, G and L), 600 nm diameter size fibres (C, H and M), 1000 nm diameter size fibres (D, I and N), and 1300 nm diameter size fibres (E, J and O) 3 (A-E), 6 (F-J) and 24 (K-O) hours after seeding. Scale bar: 100 μm.
Adhesion rate of RT4-D6P2T (P) and primary SC cells (R) are reported. Cell number is expressed as cells/mm^2± standard deviation. Spreading area of RT4-D6P2T (Q) and primary SC cells (S) 3, 6 and 24 hours after seeding. Spreading area is express as pixel area occupied by single cell ± standard deviation. Statistical analysis was carried out using one-way ANOVA. Asterisks refer to significant statistical difference with *$p \leq 0.05$, **$p \leq 0.01$ and ***$p \leq 0.001$.

3.3 Increasing fibre diameter size resulted in lower actin cytoskeleton organization and focal adhesion points presence

Both RT4-D6P2T (Fig. 3) and primary SC (Fig. 4) cultured on control condition and on 300 nm fibres displayed high actin cytoskeleton organization and focal adhesion points presence (Fig.3 A, B, F, G, K and L; Fig.4 A, B, F, G, K and L). Cells seeded on 600, 1000 and 1300 nm fibres resulted in lower actin cytoskeleton and focal adhesion points formation displaying a more elongated morphology (Fig. 3 C-E, H-J, and M-O; Fig. 4 C-E, H-J, and M-O). This trend was maintained in all the tested time points (3, 6 and 24 hours). Finally, actin cytoskeleton staining

showed that cells cultured on control condition or 300 and 600 nm fibres displayed a spread morphology in comparison to cells cultured on 1000 and 1300 nm fibres which are characterized by elongated morphology. These data are in according with adhesion assay results.

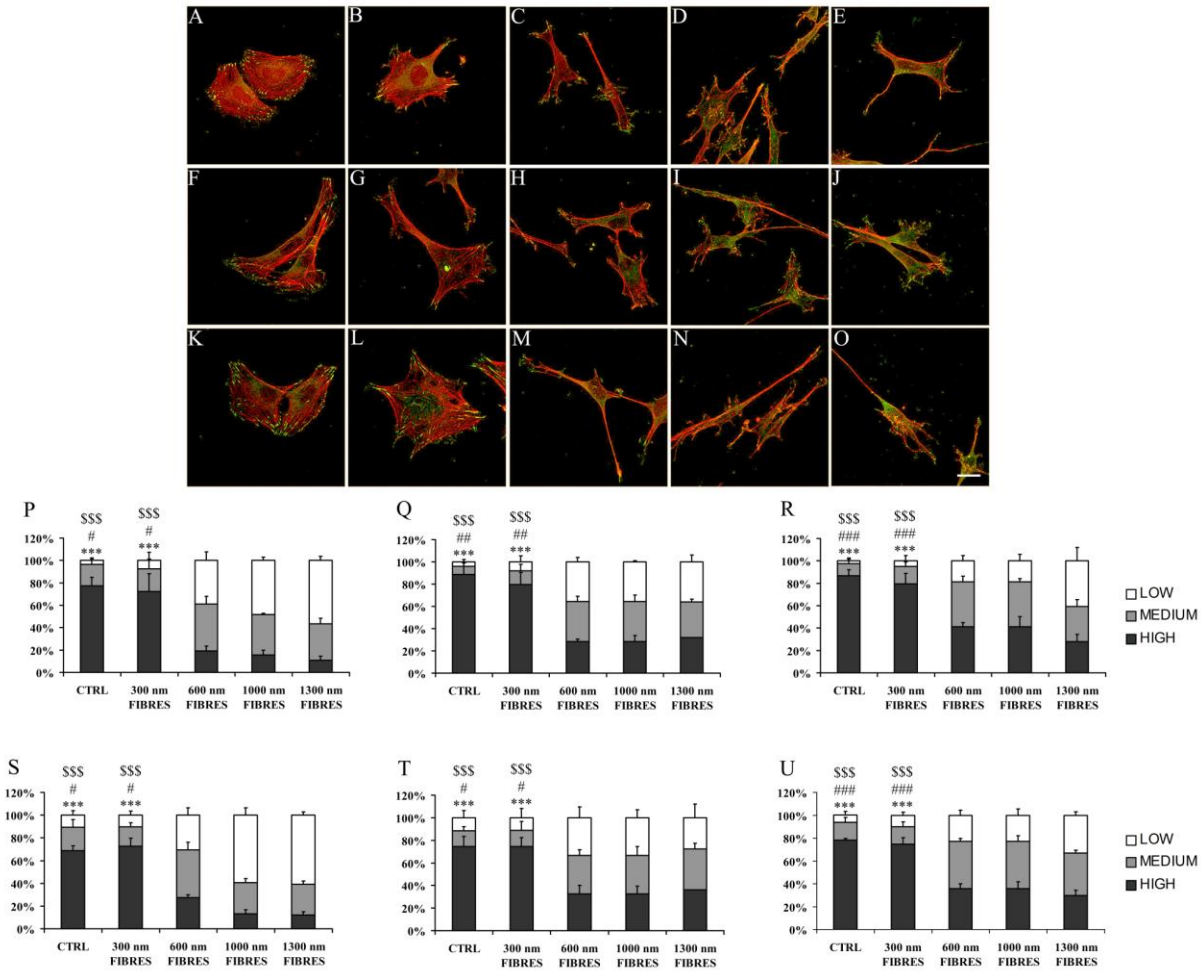

Figure 3. Actin cytoskeleton organization and focal adhesion point presence. Fluorescence images following phalloidin-actin staining (red), vinculin (green) and DAPI (blue) staining of RT4-D6P2T on poly-L-lysine coated coverslips (control condition, A, F and K), 300 nm diameter size fibres (B, G and L), 600 nm diameter size fibres (C, H and M), 1000 nm diameter size fibres (D, I and N), and 1300 nm diameter size fibres (E, J and O) 3 (A-E), 6 (F-J) and 24 (K-O) hours after seeding. Scale bar: 20 μm. Percentage of cells with low, medium or high actin cytoskeleton organization ± standard deviation 3 (P), 6 (Q) and 24 (R) hours after seeding are reported. Percentage of cells with low, medium or focal adhesion points presence ± standard deviation 3 (S), 6 (T) and 24 (U) hours after seeding are reported

Statistical analysis was carried out using one-way ANOVA with */#/$ $p \leq 0.05$, **/##/$$ $p \leq 0.01$ and ***/###/$$$ $p \leq 0.001$. Asterisks refer to statistical difference in between low actin cytoskeleton organization and focal adhesion point presence conditions. Hashes refer to statistical difference in between medium actin cytoskeleton organization and focal adhesion point presence conditions. Dollars refer to statistical difference in between medium actin cytoskeleton organization and focal adhesion point presence conditions.

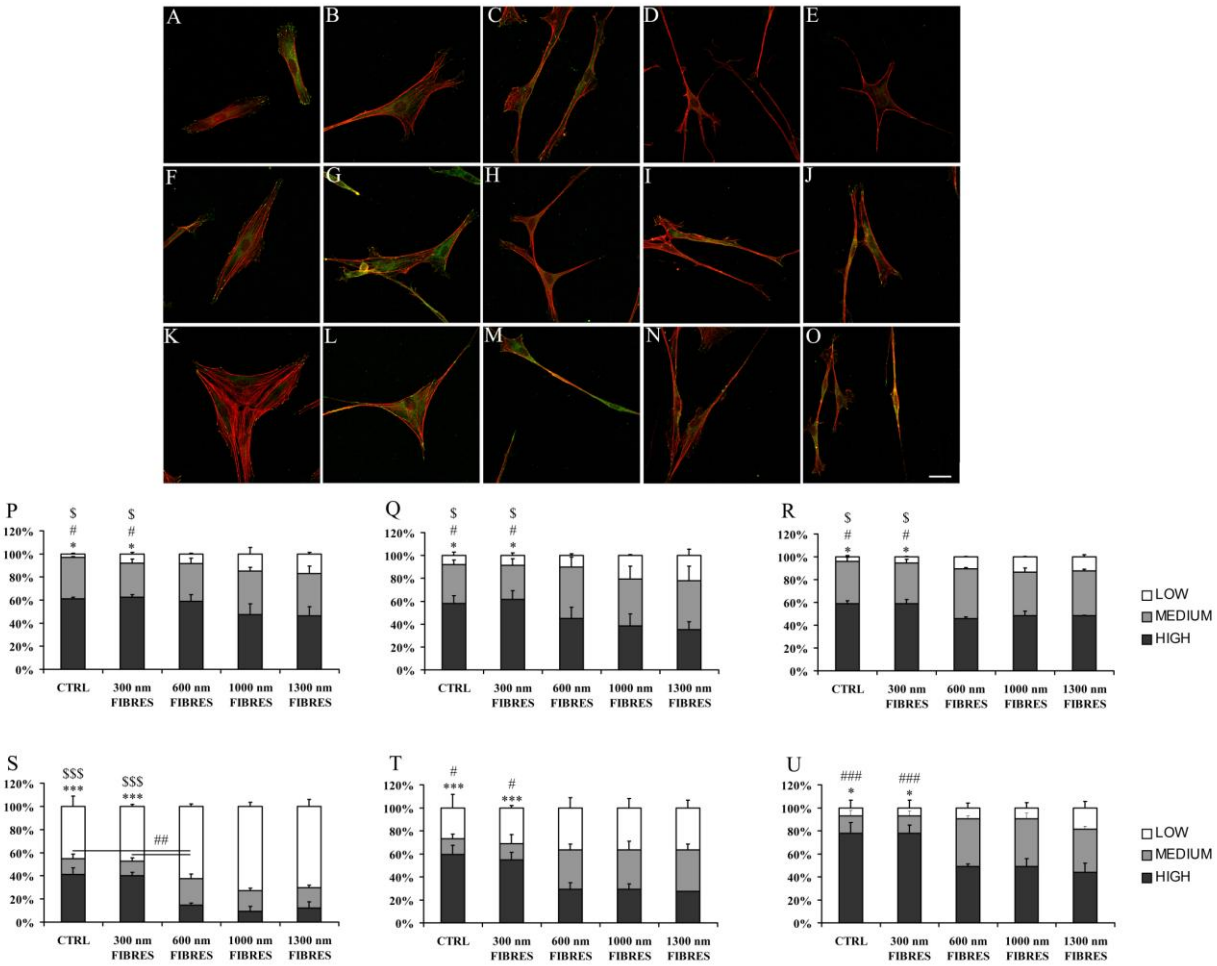

Figure 4. Actin cytoskeleton organization and focal adhesion point presence evaluation. Fluorescence images following phalloidin-actin staining (red), vinculin (green) and DAPI (blue) staining of SC primary culture on poly-L-lysine coated coverslips (control condition, A, F and K), 300 nm diameter size fibres (B, G and L), 600 nm diameter size fibres (C, H and M), 1000 nm diameter size fibres (D, I and N), and 1300 nm diameter size fibres (E, J and O) 3 (A-E), 6 (F-J) and 24 (K-O) hours after seeding. Scale bar: 20 μm. Percentage of cells with low, medium or high actin cytoskeleton organization ± standard deviation 3 (P), 6 (Q) and 24 (R) hours after seeding are reported. Percentage of cells with low, medium or focal adhesion points presence ± standard deviation M 3 (S), 6 (T) and 24 (U) hours after seeding are reported
Statistical analysis was carried out using one-way ANOVA with */#/$ $p \leq 0.05$, **/##/$$ $p \leq 0.01$ and ***/###/$$$ $p \leq 0.001$.
Asterisks refer to statistical difference in between low actin cytoskeleton organization and focal adhesion point presence conditions.
Hashes refer to statistical difference in between medium actin cytoskeleton organization and focal adhesion point presence conditions.
Dollars refer to statistical difference in between medium actin cytoskeleton organization and focal adhesion point presence conditions.

3.4 Increasing fibre diameter size results in higher filopodia formation

Lamellipodium are motile organelle defined as a thin sheet of cytoplasm filled with a branched network of actin filaments arranged in a criss-cross pattern (Fig. 5A). The width of *lamellipodium* (commonly 0.1-0.2 μm) usually does not exceed 10 μm and the actin filaments concentration decreases from the front to the back. *Filopodia* are rod-shaped cell protrusion filled with linear actin filaments and their formation often coincides with the presence of *lamellipodium*.

Filopodia can reach 50 μm length (Fig. 5B). Increasing fibre diameter size resulted in a higher number of cells displaying *filopodia* in both RT4-D6P2T (Fig. 5 C-E) and primary SC (Fig. 5 F-H).

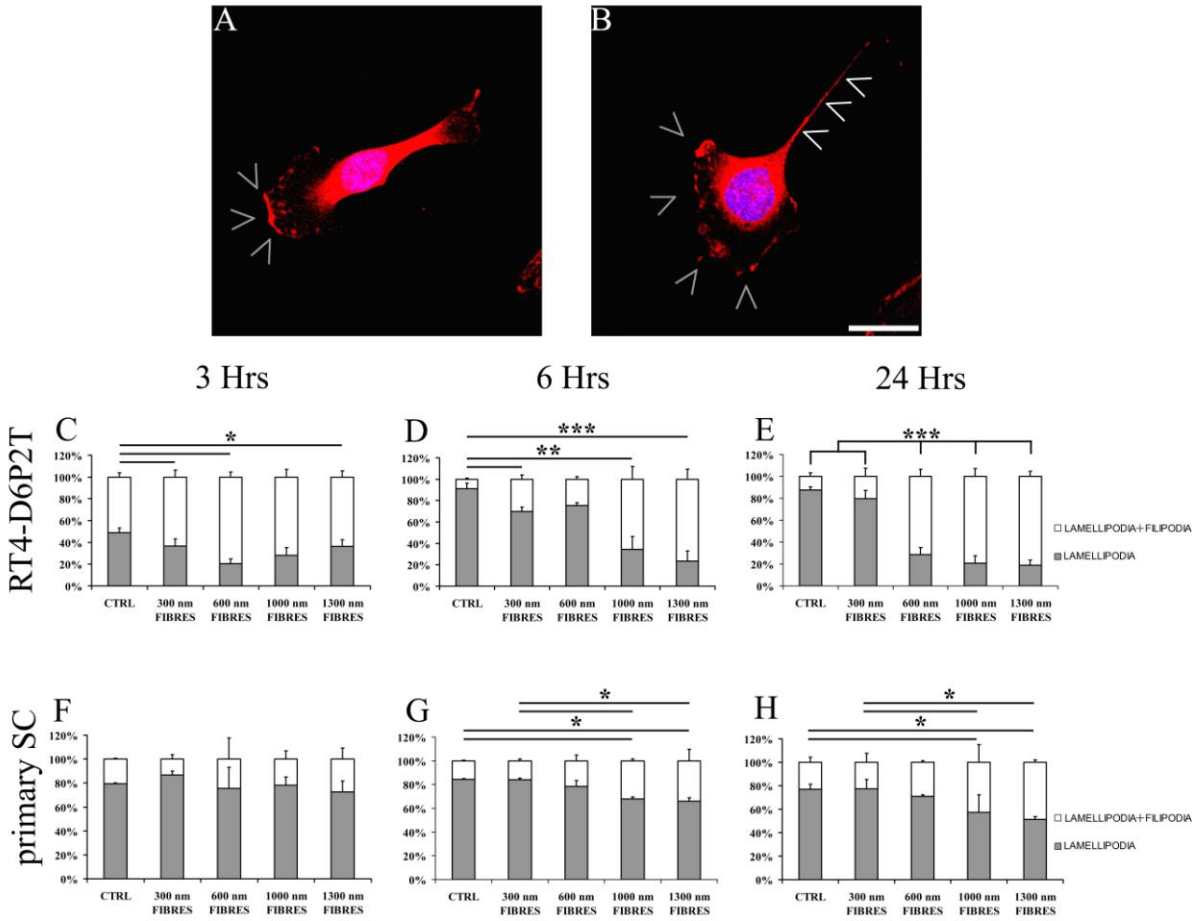

Figure 5. *Lamellipodium* and *filopodia* presence evaluation. Fluorescence images after S-100β staining (red) and DAPI (blue) staining of RT4-D6P2T. Grey arrows indicate lamellipodium protrusion (A) whereas white arrows indicate *filopodia* protrusion (A and B). Scale bar: 20 μm. Percentage of RT4-D6P2T cells characterized by *lamellipodium* and *lamellipodium* and *filopodia* protrusions 3 (C), 6 (D) and 24 (E) hours after seeding are expressed as mean ± standard deviation. Percentage of primary SC characterized by *lamellipodium* and *lamellipodium* and *filopodia* protrusion 3 (F), 6 (G) and 24 (H) hours after seeding are expressed as mean ± standard deviation. Statistical analysis was carried out using one-way ANOVA. Asterisks refer to significant statistical difference with *$p \leq 0.05$, **$p \leq 0.01$ and ***$p \leq 0.001$.

3.5 Increasing fibre diameter size resulted in higher cell motility and migration

Time lapse results showed that these is no difference in cell motility between control condition and 300 and 600 nm fibres for both RT4-D6P2T (Fig. 6A) and primary SC (Fig. 6B). By contrast, cells seeded on 1000 and 1300 nm fibres are characterized by higher motility in comparison to 300 and 600 nm fibres (Fig. 6).

As concerns three-dimensional cell migration through the fibre matrices, RT4-D6P2T cells were characterized by higher migration when seeded on 1300 nm fibres in comparison to 300 and

600 nm fibres (Fig. 7A). Primary SC seeded on 1000 and 1300 nm fibres were characterized by an higher migration rate in comparison to 300 nm fibres (Fig. 7B).

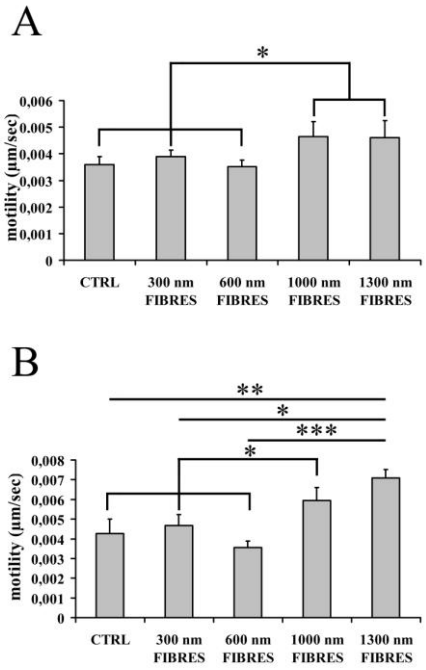

Figure 6. Bi-dimensional motility evaluation: time lapse assay. RT4-D6P2T (A) and primary SC (B) motility is express as µm/sec± standard deviation. Statistical analysis was carried out using one-way ANOVA. Asterisks refer to significant statistical difference with *p ≤ 0.05, **p ≤ 0.01 and ***p ≤ 0.001.

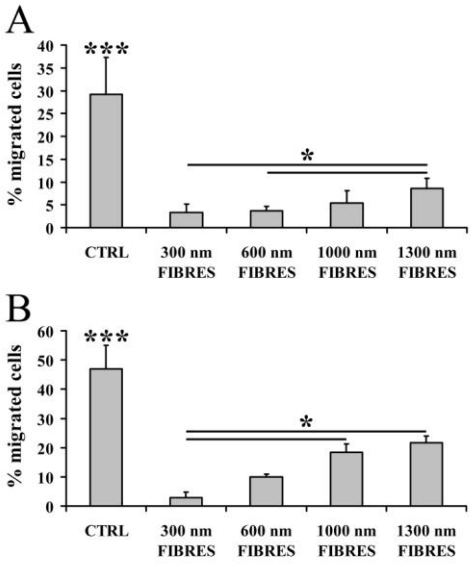

Figure 7. Three-dimensional migration evaluation: transwell assay. RT4-D6P2T (A) and primary SC (B) migration is express as percentage of migrated cells ± standard deviation. Statistical analysis was carried out using one-way ANOVA. Asterisk refers to significant statistical difference with *p ≤ 0.05, **p ≤ 0.01 and ***p ≤ 0.001.

3.6 Increasing fibre diameter size resulted in lower cell proliferation rate

Cell proliferation results show that, after 5 days, RT4-D6P2T cells displayed lower proliferation rate when seeded on 1300 nm fibres in comparison to control condition and 300, 600 and 1000 nm fibres (Fig. 8U). After 7 days, primary SC were characterized by lower proliferation rate when seeded on 600, 1000 and 1300 nm fibres in comparison to SC seeded on 300 nm fibres. Both RT4-D6P2T and primary SC cells reached confluent levels in all the tested condition.

Primary SC staining against S100β revealed normal spread morphology in all the tested time points in according with data reported in adhesion assay (Fig.8 A-T). The same results were obtained using RT4-D6P2T cell line (data not shown).

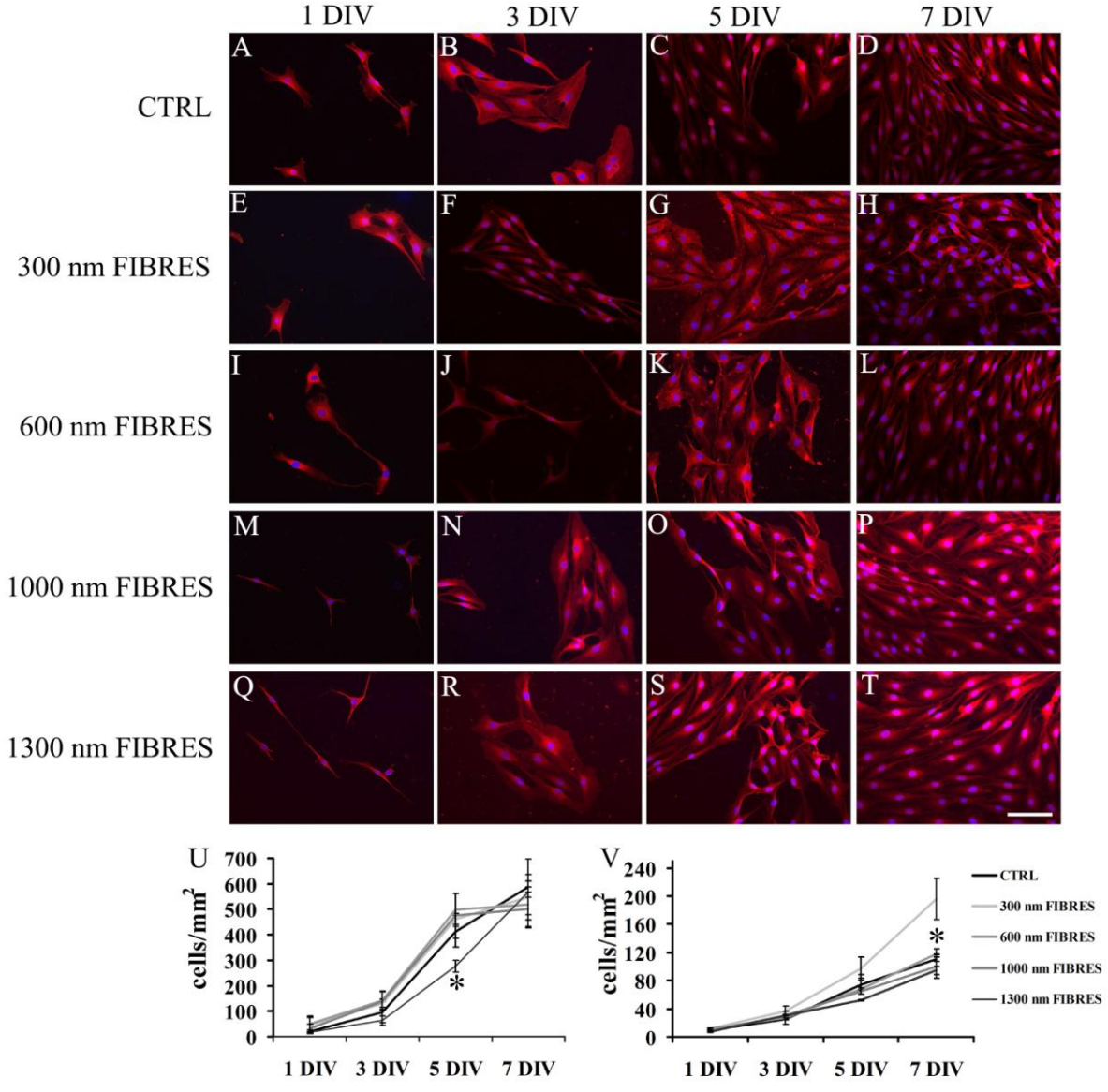

Figure 8. Proliferation assay. Fluorescence images following S100β (red) and DAPI (blue) staining of primary SC on poly-L-lysine coated coverslips (control condition, A-D), 300 nm diameter size fibres (E-H), 600 nm diameter size fibres (I-L), 1000 nm diameter

size fibres (M-P), and 1300 nm diameter size fibres after 1 (A, E, I, M and Q), 3 (B, F, J, N and R), 5 (C, G, K, O and R) and 7 (D, M, L, P and t) days *in vitro* (DIV). Scale bar: 50 μm. Proliferation rate of RT4-D6P2T (U) and primary SC cells (V) are reported. Cell number is expressed as cells/mm^2± standard deviation. Statistical analysis was carried out using one-way ANOVA. Asterisks refer to significant statistical difference with *$p \leq 0.05$, **$p \leq 0.01$ and ***$p \leq 0.001$.

3.7 Increasing fibre diameter size resulted in higher axon outgrowth

DRG explants cultured on matrigel® or fibre matrices without adding NGF in culture medium results in no axon sprouting (Fig.9 A and G). NGF addition to the culture medium resulted in axon sprouting in all the tested conditions (Fig. 9 B-F and H-L). DRG cultured on 1000 and 1300 nm fibres were characterized by an higher axon density in comparison to DRG cultured on 300 nm fibres whereas there was no difference in comparison to the positive control condition (Fig. 9M). DRGs are cultured on 1300 nm fibres displayed an higher spreading area in comparison to DRGs cultured on 300 nm fibres. These data are in according with axon density measurements (Fig. 9N). DRG explants culture resulted in a lower axon length when DRGs were cultured on 300 nm fibres in comparison to DRGs cultured on 600, 1000 and 1300 nm fibres (Fig. 9O).

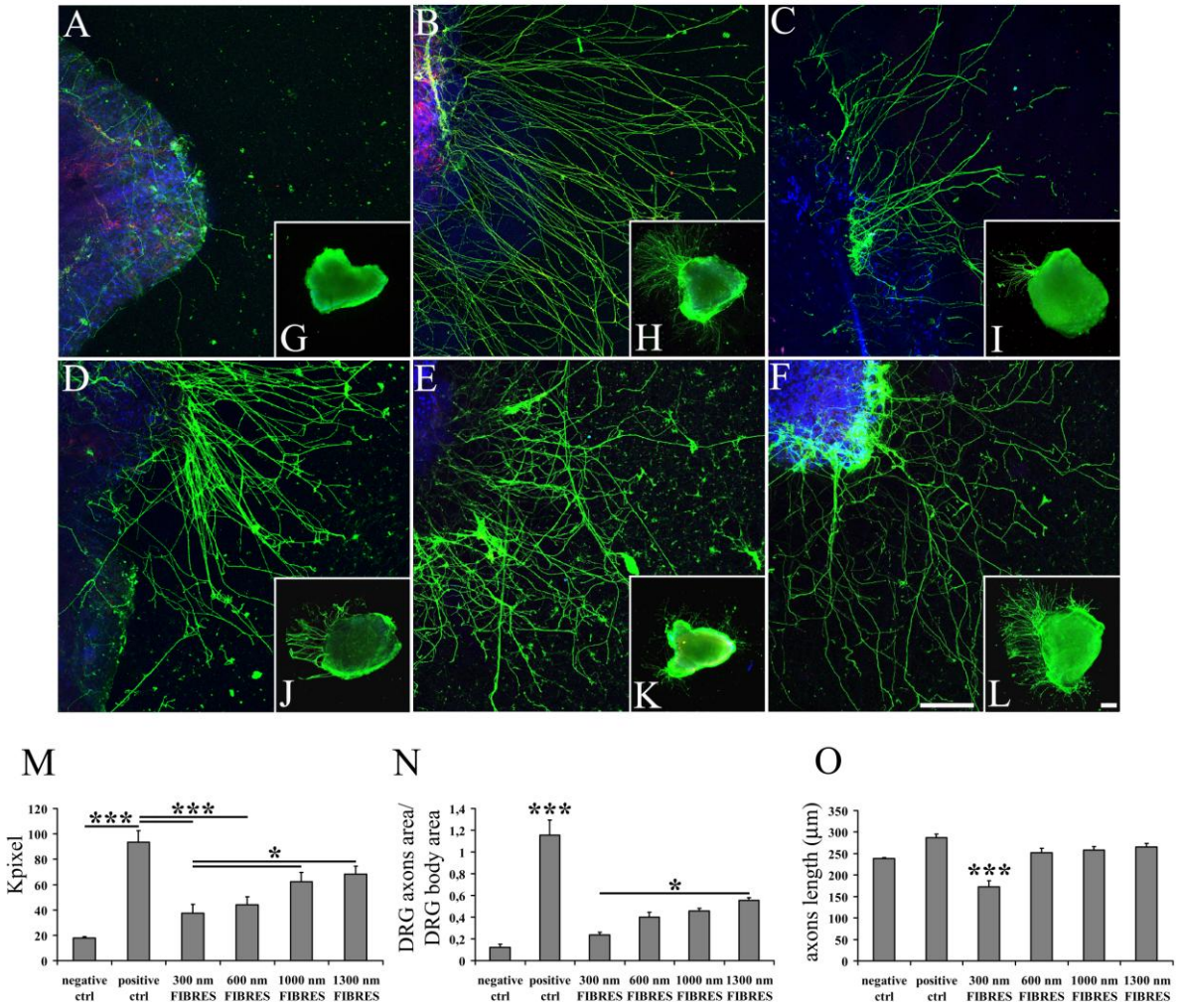

Figure 9. DRG axon outgrowth assay. Fluorescence images after β-tubulin (green) and DAPI (blue) staining of DRG explants cultured on matrigel® coated coverslips without NGF (negative control condition, A and G), matrigel® coated coverslips with 50 ng of NGF/ml of medium (positive control condition, B and H), 300 nm diameter size fibres (C and I), 600 nm diameter size fibres (D and J), 1000 nm diameter size fibres (E-K), and 1300 nm diameter size fibres (F-L). Confocal detailed images (A-F) and fluorescence microscope images of the whole explants are reported (G-L). Scale bar: 20 µm. Axon density expressed as Kpixel ± standard deviation (M), sprouting area expressed as DRG axon area/DRG axon area ratio ± standard deviation (N) and axon length expressed as µm ± standard deviation (O) are reported. Statistical analysis was carried out using one-way ANOVA. Asterisks refer to significant statistical difference with *$p \leq 0.05$, **$p \leq 0.01$ and ***$p \leq 0.001$.

4. DISCUSSION

For tissue engineering applications, the distribution and growth of cells on a scaffold are key requirements. A number of studies demonstrates that micro-to-nano-scale topography plays an important role in controlling cell adhesion, survival, proliferation and differentiation [13, 14, 16, 18,

20]. As concerning peripheral nerves, the development of an artificial biomaterial scaffold mimicking its native structure is important to improve peripheral nerve regeneration [6, 14, 28]. In particular, the regeneration phase needs an appropriate basal lamina which mediates the contact between migratory SC and regenerating axon [2, 44, 45].

A major problem in the generation of artificial scaffold mimicking extracellular matrix and basal lamina is to the use of native adhesion substrates for scaffolds preparation since they are animal derived materials and may cause immune rejection [4, 38, 46]. Gelatin, a natural polymer obtained by thermal denaturation of collagen, is becoming widely used in biomimetic tissue engineering scaffolds preparation because of its low immunogenicity [38, 46].

Adequate fibrous substrates, functioning as an extracellular matrix, can be easily prepared by electrospinning, which allows to obtain random or aligned fibrous matrices suitable as internal filler for nerve guidance channels [31]. In particular, in a previously published study [39], authors reported that electrospun gelatin fibres can be prepared dissolving gelatin in water solution and using GPTMS as gelatin crosslinker. GPTMS crosslinked gelatin nano-fibres result in substrates displaying high biocompatibility towards neural tissue and suitable biodegradation rate [39].

In this work, different kinds of nano- and micro-fibres were successfully prepared by electrospinning technique by adjusting gelatin solution concentration and flow rate. Resulting nano-fibres displayed a diameter size ranging from 300 nm to 600 nm, whereas fibre diameter size of micro-fibres was in the range of 1-1.3 μm. Nano-fibres (300 nm) are characterized by lower porosity and a more intricate network [30, 47-49].

In agreement with our previous study [39], we here provide further evidence on the biocompatibility of gelatin electrospun, in particular with respect to SCs that are the key element in peripheral nerve regeneration [50].

In addition, results of this study provide several original pieces of information about the influence of fibre diameter size on neural tissue organization and morphology. The different fibre diameter size may results in a diverse three-dimensional scaffold architecture and porosity (distance

between fibres) influencing cell organization by providing different substrate mechanical properties (stiffness and elasticity) and focal adhesions (FAs) patterns [48, 51, 52].

As concerning the mechanical properties, has been reported that soft hydrogels favour neurons survival whereas harder gels promote glial cultures. Moreover, soft gels inhibit cell spreading, self-renewal, and differentiation [52, 53]. Another study reported that mesenchymal stem cells are sensitive to tissue elasticity particularly, soft matrices that mimick brain are neurogenic whereas stiffer matrices that mimic muscle are myogenic suggesting that matrix physical properties play a key role in cell lineage commitment [51].

The mechanical interaction of cells and their cytoskeleton with ECM proteins results in the activation of a variety of biological processes. A complex interplay between FAs and actin cytoskeleton leas to the generation of membrane protrusion (*lamellipodium* and *filopodia*) and traction forces regulating cell shape, proliferation, motility and migration [30, 49, 54, 55]. Focal adhesion kinase (FAK) is a central protein in focal adhesions points formation by interacting with integrins, paxillin, α-actinin and other proteins that link FAs to the actin cytosketon it regulates several cytoskletal and other focal adhesion proteins influencing cell motility, migration, morphology and contractility [47, 48, 54, 55]. FAK can be activated by ECM components (through integrins) resulting in its tyrosine phosphorilation. FAK phosphorilation give rise to the activation of several pathways such as: Ras/Raf/MEK/Erk1-2 witch regulate cell proliferation; Paxilin/Crk/Rac witch regulate cytoskeleton reorganization and cell motility and migration; PI3K pathway witch regulate cell survival [29, 54, 55].

Results showed that SCs on gelatin nano-fibres displayed a spread morphology whereas when SC are cultured on micro-fibres they are characterized by a more elongated shape in according to literature data [56]. These results are in according with literature data in which aminated nano-fiber meshes have been showed to support an higher degree of cell adhesion compared to aminated films [16]. In addition, SC cultured on micro-fibres displayed a stretched shape with elongated actin filaments and lower focal adhesions points formation organized at the cell extremities. The different

SC spread morphology on nano-fibres may be due to the intricate network between fibres that provides an higher number of focal adhesions points in comparison to micro-fibres [12]. The assessment of actin filaments organization, i.e. the so called stress fibres [30, 48], provides a possible explanation of the observed difference in cell morphology by showing that actin stress fibres are differently organized depending on gelatin fibres size with a criss-cross arrangement on nano-fibres. This occurrence that can be attributed to the higher fibre matrix density of nano-fibres [12, 32] is suitable to be at the basis of their spread morphology [12, 13]. These data are in according with another study in which has been reported that FAK-deficient cells display a rounded morphology with a smaller spreading area, a pronounced actin cytoskeleton cortical distribution and loss of stress fibres [54, 57, 58]. On the other hand FAK rescue results in larger spreading area and stress fibres reformation this can be due to the correct FAs pattern formation [54, 57].

The formation of *lamellipodia* is associated with important actin filament polymerization and stress fibres formation [30, 47, 55]. Since we observed a difference in FAs pattern and actin organization between cells seeded on nano-fibres in comparison to cells seeded on micro-fibres we focused our attention on *lamellipodium* and *filopodia* formation. These structures are known to be involved in SC migration and axon outgrowth [6, 10, 49, 59] as well as myelination [60, 61]. *Filipodia* often originate from *lamellipodium* protrusion and have an important role in cell migration and axon outgrowth [27, 30, 49, 60, 61]. Our results showed that the number of SC presenting *filipodia* is higher when these cells are cultured on micro-fibres in comparison to nano-fibres. The constant remodelling of the actin cytoskeleton into *filopodia*, *lamellipodia*, and stress fibres is essential for cell migration [30, 47, 55]. Altogether the previous discussed data suggest that micro-fibres substrates lead to an higher motility and migration behaviour. The pro-migratory effect of micro-fibres was confirmed by bi-dimensional and three-dimensional migration assays which showed that micro-fibres promote higher cell motility and migration in comparison to nano-fibres. These results are in agreement with a previous *in vitro* study which showed that a combination of micro-and nano-fibres improves cell migration in comparison to nano-fibres alone [62].

Finally, actin reorganization and stress fibres remodelling participate to cell division process (cell proliferation) [30, 47]. Our results showed that micro-fibres resulted in lower SC proliferation rate in comparison to nano-fibres substrates. This effect can be due to the FAs pattern and lower stress fibres organization presented by SC cultured on micro-fibers substrate and to the mechanical properties of the fibres in according to literature data discussed before [51-53]. Our data are in according with a study in which neural stem/progenitor cells displayed fibres higher degree of proliferation and cell spreading and lower degree of cell aggregation as the fibre diameter decreased [23].

Altogether these results suggest that the mechanical properties and the topographical organization of the electrospun gelatin fibres influence SC morphology, organization, migration and proliferation by acting on the FAs pattern and stress fibres polymerization in according to the previous discussed literature data [16, 23, 48, 51-54, 57, 58].

Finally, since both SC and re-growing axons play a key role in nerve regeneration [50], axon outgrowth on the different substrates was tested by culturing and stimulating DRG explants. DRG explants revealed higher axon sprouting if cultured on micro-fibres in comparison to nano-fibres substrates, an occurrence that can have a negative impact on *in vivo* regeneration since excessive sprouting could result in aberrant regeneration [63, 64]. Controversially to our results, other studies demonstrates that align nano-fibres significantly promotes neuronal differentiation, axonal outgrowth and cell viability in comparison to align micro-fibres [27, 56, 65]. Moreover, DRG explants cultured on both align nano- and micro-fibres displayed an higher axonal density and length in comparison to random fibres [56, 65]. Although, the previous discussed data used different fibre diameter range (400-800 nm) and cell models such as human embryonic stem cell, central nervous system neurons and astrocytes which may display a different *in vitro* behaviour in comparison to peripheral nervous system cells. On the other hand, another work showed that axonal sprouting and maturation following rat sciatic nerve repair with conduit containing align or align/ random nano-fibres was closed to isograft condition [25]. On the basis of our *in vitro* an *ex vivo*

results, it would be interesting to test *in vivo* the effect of a nerve guidance conduit filled with align fibres in combination with random fibres displaying different diameter size.

For peripheral nerve regeneration applications an ideal biomimetic material should promote cell proliferation and adhesion as well as migration and axon outgrowth [6, 10, 50]. Recent studies reported that nano-fibres improved functional recovery after rat sciatic nerve repair [25, 66] suggesting, that proliferation- and adhesion-promoting substrates are more important in the perspective of promoting peripheral nerve regeneration *in vivo*.

5. CONCLUSION

This study point up the possibility of producing GPTMS-cross-linked gelatine random fibres of different diameter size by electrospinning technique. The use of fibres displaying a different topography can be used *in vitro* and *ex vivo* to modulate Schwann cells and axons behaviour.

In according with the previous study we confirmed that the prepared electrospun random fibres ranging from nano-meter to micro-meter size display biocompatible and biomimetic properties in relation to the main cell components of the peripheral nerve Schwann cells and axons.

In this study we showed that random fibre size affects both SC and axon behaviour. In particular, electrospun micro-fibres promote Schwann cell migration and axonal outgrowth whereas electrospun nano-fibres promote Schwann cell proliferation and adhesion.

Further *in vivo* investigations will be performed to analyze the influence of the random fibre size on promoting peripheral nerve regeneration. The probable conduit design will consist of an outer porous structure made of poly(ε-caprolactone) and polyethylene oxide 60/40 wt/wt blend which should ensure nutrient permeation and avoids fibroblast infiltration inside the tube. In order to promote Schwann cells migration and differentiation and directional axon ingrowths the conduit core will consist of an inner layer composed random fibres and an inner layer of gelatine aligned fibres. The inner layer of aligned fibres should influence Schwann cells migration and oriented organization and promote axonal growth parallel to the aligned fibres. On the other hand the

different fibre topography (size composition) of the outer conduit layer should inhibit scar tissue formation and influence Schwann cells differentiation and axon growth density. Thus, the employ of fibres displaying a different topography in different combination ration might be use to modulate SC and axonal behaviour *in vivo* in order to achieve better peripheral nerve regeneration.

6. ACKNOWLEDGEMENTS

This work was supported by grants from Compagnia di San Paolo (MOVAG) and the University of Torino.

7. REFERENCES

[1] X. Gu, F. Ding, Y. Yang, J. Liu, Prog Neurobiol, 93 (2011) 204-230.
[2] S. Ichihara, Y. Inada, T. Nakamura, Injury, 39 Suppl 4 (2008) 29-39.
[3] X. Jiang, S.H. Lim, H.Q. Mao, S.Y. Chew, Exp Neurol, 223 (2010) 86-101.
[4] M. Siemionow, G. Brzezicki, Int Rev Neurobiol, 87 (2009) 141-172.
[5] E. Biazar, M.T. Khorasani, N. Montazeri, K. Pourshamsian, M. Daliri, M. Rezaei, M. Jabarvand, A. Khoshzaban, S. Heidari, M. Jafarpour, Z. Roviemiab, Int J Nanomedicine, 5 (2010) 839-852.
[6] R. Deumens, A. Bozkurt, M.F. Meek, M.A. Marcus, E.A. Joosten, J. Weis, G.A. Brook, Prog Neurobiol, 92 (2010) 245-276.
[7] S. Geuna, S. Gnavi, I. Perroteau, P. Tos, B. Battiston, Int Rev Neurobiol, 108 (2013) 35-57.
[8] S. Geuna, S. Nicolino, S. Raimondo, G. Gambarotta, B. Battiston, P. Tos, I. Perroteau, Microsurgery, 27 (2007) 429-438.
[9] W.W. Campbell, Clin Neurophysiol, 119 (2008) 1951-1965.
[10] G.C. de Ruiter, M.J. Malessy, M.J. Yaszemski, A.J. Windebank, R.J. Spinner, Neurosurg Focus, 26 (2009) E5.
[11] M.B. Steed, V. Mukhatyar, C. Valmikinathan, R.V. Bellamkonda, Atlas Oral Maxillofac Surg Clin North Am, 19 (2011) 119-130.
[12] S. Agarwal, J.H. Wendorff, A. Greiner, Polymer, 49 (2008) 5603-5621.
[13] L. Bacakova, E. Filova, M. Parizek, T. Ruml, V. Svorcik, Biotechnol Adv, 29 (2011) 739-767.
[14] A.G. Harvey, E.W. Hill, A. Bayat, Expert Rev Med Devices, 10 (2013) 257-267.
[15] D.E. Birk, R.L. Trelstad, J Cell Biol, 99 (1984) 2024-2033.
[16] K.N. Chua, C. Chai, P.C. Lee, Y.N. Tang, S. Ramakrishna, K.W. Leong, H.Q. Mao, Biomaterials, 27 (2006) 6043-6051.
[17] J. Hu, X. Liu, P.X. Ma, Biomaterials, 29 (2008) 3815-3821.
[18] M.J. Dalby, D. McCloy, M. Robertson, H. Agheli, D. Sutherland, S. Affrossman, R.O. Oreffo, Biomaterials, 27 (2006) 2980-2987.
[19] A. Hart, N. Gadegaard, C.D. Wilkinson, R.O. Oreffo, M.J. Dalby, J Mater Sci Mater Med, 18 (2007) 1211-1218.
[20] M.J. Dalby, N. Gadegaard, R. Tare, A. Andar, M.O. Riehle, P. Herzyk, C.D. Wilkinson, R.O. Oreffo, Nat Mater, 6 (2007) 997-1003.
[21] J.B. Recknor, D.S. Sakaguchi, S.K. Mallapragada, Biomaterials, 27 (2006) 4098-4108.
[22] K.S. Rho, L. Jeong, G. Lee, B.M. Seo, Y.J. Park, S.D. Hong, S. Roh, J.J. Cho, W.H. Park, B.M. Min, Biomaterials, 27 (2006) 1452-1461.

[23] G.T. Christopherson, H. Song, H.Q. Mao, Biomaterials, 30 (2009) 556-564.
[24] D. Gupta, J. Venugopal, M.P. Prabhakaran, V.R. Dev, S. Low, A.T. Choon, S. Ramakrishna, Acta Biomater, 5 (2009) 2560-2569.
[25] W. Wang, S. Itoh, K. Konno, T. Kikkawa, S. Ichinose, K. Sakai, T. Ohkuma, K. Watabe, J Biomed Mater Res A, 91 (2009) 994-1005.
[26] Y.C. Huang, S.H. Hsu, W.C. Kuo, C.L. Chang-Chien, H. Cheng, Y.Y. Huang, J Biomed Mater Res A, 99 (2011) 86-93.
[27] J. Xie, M.R. MacEwan, X. Li, S.E. Sakiyama-Elbert, Y. Xia, ACS Nano, 3 (2009) 1151-1159.
[28] M.B. Rahmany, M. Van Dyke, Acta Biomater, 9 (2013) 5431-5437.
[29] P. Defilippi, C. Olivo, M. Venturino, L. Dolce, L. Silengo, G. Tarone, Microsc Res Tech, 47 (1999) 67-78.
[30] P.K. Mattila, P. Lappalainen, Nat Rev Mol Cell Biol, 9 (2008) 446-454.
[31] N. Bhardwaj, S.C. Kundu, Biotechnol Adv, 28 (2010) 325-347.
[32] J. Venugopal, S. Low, A.T. Choon, S. Ramakrishna, J Biomed Mater Res B Appl Biomater, 84 (2008) 34-48.
[33] W. Liu, S. Thomopoulos, Y. Xia, Adv Healthc Mater, 1 (2012) 10-25.
[34] M.P. Prabhakaran, J.R. Venugopal, T.T. Chyan, L.B. Hai, C.K. Chan, A.Y. Lim, S. Ramakrishna, Tissue Eng Part A, 14 (2008) 1787-1797.
[35] J. Venugopal, S. Ramakrishna, Tissue Eng, 11 (2005) 847-854.
[36] C. Cunha, S. Panseri, S. Antonini, Nanomedicine, 7 (2011) 50-59.
[37] D. Liang, B.S. Hsiao, B. Chu, Adv Drug Deliv Rev, 59 (2007) 1392-1412.
[38] G. Ciardelli, V. Chiono, Macromol Biosci, 6 (2006) 13-26.
[39] C. Tonda-Turo, E. Cipriani, S. Gnavi, V. Chiono, C. Mattu, P. Gentile, I. Perroteau, M. Zanetti, G. Ciardelli, Mater Sci Eng C Mater Biol Appl, 33 (2013) 2723-2735.
[40] S. Zhang, Y. Huang, X. Yang, F. Mei, Q. Ma, G. Chen, S. Ryu, X. Deng, J Biomed Mater Res A, 90 (2009) 671-679.
[41] Y.Z. Zhang, J. Venugopal, Z.-M. huang, C.T. Lim, S. Ramakrishna, Polymer, 47 (2006) 2911-2917.
[42] A. Gilardino, S. Farcito, P. Zamburlin, C. Audisio, D. Lovisolo, J Neurosci Res, 87 (2009) 2951-2962.
[43] P. Zamburlin, A. Gilardino, S. Dalmazzo, P. Ariano, D. Lovisolo, J Neurosci Res, 84 (2006) 505-514.
[44] C. Ide, Neurosci Res, 25 (1996) 101-121.
[45] P.C. Letourneau, M.L. Condic, D.M. Snow, J Neurosci, 14 (1994) 915-928.
[46] V. Chiono, C. Tonda-Turo, G. Ciardelli, Int Rev Neurobiol, 87 (2009) 173-198.
[47] R.D. Mullins, S.D. Hansen, Curr Opin Cell Biol, 25 (2013) 6-13.
[48] J.T. Parsons, A.R. Horwitz, M.A. Schwartz, Nat Rev Mol Cell Biol, 11 (2010) 633-643.
[49] K. Rottner, T.E. Stradal, Curr Opin Cell Biol, 23 (2011) 569-578.
[50] S. Geuna, S. Raimondo, G. Ronchi, F. Di Scipio, P. Tos, K. Czaja, M. Fornaro, Int Rev Neurobiol, 87 (2009) 27-46.
[51] A.J. Engler, S. Sen, H.L. Sweeney, D.E. Discher, Cell, 126 (2006) 677-689.
[52] K. Saha, A.J. Keung, E.F. Irwin, Y. Li, L. Little, D.V. Schaffer, K.E. Healy, Biophys J, 95 (2008) 4426-4438.
[53] N.D. Leipzig, M.S. Shoichet, Biomaterials, 30 (2009) 6867-6878.
[54] B. Fabry, A.H. Klemm, S. Kienle, T.E. Schaffer, W.H. Goldmann, Biophys J, 101 (2011) 2131-2138.
[55] S.K. Mitra, D.A. Hanson, D.D. Schlaepfer, Nat Rev Mol Cell Bio, 6 (2005) 56-68.
[56] J.W. Qu, D. Wang, H. Dong, Y. Zhang, F. Zuo, B. Zhang, H. , J Biomed Mater Res Part A 101A (2013) 2667–2678.
[57] B.H. Chen, J.T.C. Tzen, A.R. Bresnick, H.C. Chen, J Biol Chem, 277 (2002) 33857-33863.

[58] X.D. Ren, W.B. Kiosses, D.J. Sieg, C.A. Otey, D.D. Schlaepfer, M.A. Schwartz, J Cell Sci, 113 (2000) 3673-3678.
[59] J. Xie, M.R. MacEwan, A.G. Schwartz, Y. Xia, Nanoscale, 2 (2010) 35-44.
[60] J.R. Chan, J Cell Biol, 177 (2007) 953-955.
[61] F. Jin, B. Dong, J. Georgiou, Q. Jiang, J. Zhang, A. Bharioke, F. Qiu, S. Lommel, M.L. Feltri, L. Wrabetz, J.C. Roder, J. Eyer, X. Chen, A.C. Peterson, K.A. Siminovitch, Development, 138 (2011) 1329-1337.
[62] K.T. Shalumon, K.P. Chennazhi, H. Tamura, K. Kawahara, S.V. Nair, R. Jayakumar, IET Nanobiotechnol, 6 (2012) 16-25.
[63] R. Eggers, F. de Winter, S.A. Hoyng, K.C. Roet, E.M. Ehlert, M.J. Malessy, J. Verhaagen, M.R. Tannemaat, PLoS One, 8 (2013) e71076.
[64] A. Shakhbazau, C. Mohanty, D. Shcharbin, M. Bryszewska, A.M. Caminade, J.P. Majoral, J. Alant, R. Midha, J Control Release, 172 (2013) 841-851.
[65] J.Y. Wang, R. Wei, Y. Wang, H. Xu, X. Zhang, H., J. Biomed Mater Res Part A, 100A (2012) 632-645.
[66] X. Jiang, R. Mi, A. Hoke, S.Y. Chew, J Tissue Eng Regen Med, (2012).